Thin Solid Films 517 (2009) 2623–2626

Contents lists available at ScienceDirect

Thin Solid Films

journal homepage: www.elsevier.com/locate/tsf

Epitaxial (Pb,La)(Zr,Ti)O_3 thin films on buffered Si(100) by on-axis radio frequency magnetron sputtering

Ø. Nordseth *, T. Tybell, J.K. Grepstad

Department of Electronics and Telecommunications, Norwegian University of Science and Technology (NTNU), NO-7491 Trondheim, Norway

ARTICLE INFO

Article history:
Received 14 January 2008
Received in revised form 26 September 2008
Accepted 14 October 2008
Available online 25 October 2008

Keywords:
Epitaxy
Sputtering
X-ray diffraction
X-ray photoelectron spectroscopy

ABSTRACT

In this study, we discuss the case for integration of epitaxial (Pb,La)(Zr,Ti)O_3 (PLZT) thin films with silicon for electro-optic device applications. PLZT films, approximately 500 nm thick, were grown by on-axis radio frequency magnetron sputtering on CeO_2/YSZ-buffered Si(100) substrate with a $SrRuO_3$ electrode layer embedded between CeO_2 and PLZT. The structural properties and surface topography of the different oxide layers were examined with X-ray diffraction analysis and atomic force microscopy. The perovskite thin films were predominantly (001)-oriented, with a (002) rocking curve halfwidth of approximately 0.3° and a surface roughness compatible with requirements for application in optical devices. The PLZT cation stoichiometry was assessed from quantitative X-ray photoelectron spectroscopy. These measurements uncovered a substantial depletion of lead in the film surface for layers deposited at substrate temperatures above ~600 °C, whereas the surface concentration of La, Zr and Ti remained virtually unaffected over a wide range of growth temperatures.

© 2008 Elsevier B.V. All rights reserved.

1. Introduction

In order to meet the increasing demand for high performance, low-cost integrated circuits in optical communication systems, introduction of materials with versatile functional properties is being explored [1–6]. The ferroelectric perovskite (Pb,La)(Zr,Ti)O_3 (PLZT) offers several functional properties attractive to optical device applications, such as a large electro-optic coefficient and high transparency at optical frequencies [7]. The electro-optic properties of PLZT are mainly governed by the chemical composition. The PLZT target used in the present study was $(Pb_{1-x},La_x)(Zr_y,Ti_{1-y})O_3$, with $x=0.08$ and $y=0.4$, which exhibits tetragonal ferroelectric phase at room temperature and linear (Pockels) electro-optic characteristics [8]. This composition renders hysteresis loops of high coercivity and linear electro-optic response for applied fields below the coercive field. Such characteristics near zero applied field are considered attractive for optical devices operating without a biasing field, such as light modulators.

The properties of ferroelectric perovskite thin films are strongly dependent on the crystalline structure. In order to facilitate epitaxial growth of PLZT on Si(100), a buffer layer structure of CeO_2 and yttria-stabilized zirconia (YSZ) is commonly adopted [9–11]. Moreover, to add functionality to this thin film stack, a layer of $SrRuO_3$ is interposed between CeO_2 and PLZT [12]. The metallic properties of $SrRuO_3$ provide an electrode for subsequent polarization of the PLZT film. The perovskite structure of $SrRuO_3$ ensures an epitaxial relationship between this layer and PLZT.

For applications of PLZT in optical devices, it is essential that highly crystalline and uniform films can be prepared with sufficient thickness to support propagation of optical modes. A number of deposition techniques were adopted to this end, such as chemical solution processing [13], pulsed laser ablation [14], metal-organic chemical vapor deposition [15], ion beam sputtering [16], magnetron sputtering [17], spin-coating pyrolysis [18], and sol–gel processing [19]. In the present communication, we report on deposition of epitaxial (Pb,La)(Zr,Ti)O_3 thin films on buffered Si(100) using radio frequency (rf) magnetron sputtering. An on-axis target geometry was adopted in order to attain high deposition rates, compared to that for films deposited by off-axis sputtering in a preceding growth effort [20]. Deposition of homogeneous films with several hundred nanometer thickness, required for application in integrated optics, is demonstrated. Moreover, it is shown that the cation stoichiometry of such films, notably their lead content, depends critically on the substrate temperature during growth.

2. Experimental details

Buffer layers of YSZ (13 mol% Y_2O_3) and CeO_2 were initially deposited on n-type Si(100) wafers (Siltronix) by electron beam evaporation. The silicon wafers were one-sided polished, with a thickness of 350 μm and resistivity 2–20 Ω cm. A 200 nm thick titanium layer was predeposited on the reverse of the polished silicon wafers to allow for radiative heating of the substrate during oxide film

* Corresponding author.
E-mail address: ornulf.nordseth@iet.ntnu.no (Ø. Nordseth).

0040-6090/$ – see front matter © 2008 Elsevier B.V. All rights reserved.
doi:10.1016/j.tsf.2008.10.038

growth. The wafers were cut in 20×20 mm^2 dies, which were cleaned ultrasonically in acetone and subsequently rinsed with isopropanol. The substrates were heated in high vacuum at 800 °C in a multi-target e-beam evaporation chamber. YSZ and CeO_2 buffer layers were grown on the polished Si(100) surface at a partial oxygen pressure of 1×10^{-4} mbar, without removing the native oxide and without breaking the vacuum between deposition of the two oxide layers. The introduction of oxygen in the evaporation chamber at the initial stage of YSZ deposition was delayed by ~30 s, in order to allow for dissociated Zr ions to reduce the native surface SiO_x layer [21,22]. The growth rate was approximately 0.3 nm/s for both layers, with typical thicknesses of 40 and 10 nm for CeO_2 and YSZ, respectively. These CeO_2/YSZ-buffered Si(100) substrates were then subdivided into 5×5 mm^2 dies and rinsed in acetone and isopropanol.

PLZT and $SrRuO_3$ thin films were deposited on the buffered Si(100) substrates by on-axis and off-axis rf magnetron sputtering, respectively. For epitaxial growth of PLZT the buffered substrates were radiatively heated to temperatures in the range 500–750 °C, as measured with an optical pyrometer. The films were grown in a mixed atmosphere of oxygen and argon (O_2/Ar=4:10) at a total pressure of 100 mTorr. The separation between the 3-inch $Pb_{1.104}La_{0.08}Zr_{0.4}Ti_{0.6}O_3$ target (Praxair Surface Technologies) and the substrate was 48 mm, with a corresponding deposition rate of approximately 2.5 nm/min. The PLZT target contained 20 mol% excess lead, to compensate for non-stoichiometric transfer of lead in the sputter deposition process. The $SrRuO_3$ layer was deposited at a substrate temperature of approximately 810 °C, a total pressure of 175 mTorr, and an O_2/Ar ratio of 4:9. The PLZT films were grown both directly on CeO_2/YSZ-buffered Si(100) and with $SrRuO_3$ embedded in the multilayer stack. The growth conditions for PLZT were the same in both cases.

X-ray diffraction measurements were performed in order to establish the phase and crystalline orientation of the different layers, using a Bruker D8 Discover X-ray diffractometer. The topography of the film surface was examined by tapping mode atomic force microscopy (AFM), using a Veeco MultiMode V scanning probe microscope. In order to determine the elemental composition of the PLZT films, quantitative X-ray photoelectron spectroscopy (XPS) analysis was carried out using a VG Escalab MkII system equipped with an Al/Mg twin anode and a hemispherical electron energy analyzer. The electron scattering length in these measurements renders a sampling depth of 2.0 ± 0.5 nm for this material [23]. The recorded peak energies were corrected for electrostatic sample charging by assigning a C1s core level binding energy of 285.0 eV to emission from adventitious surface carbon.

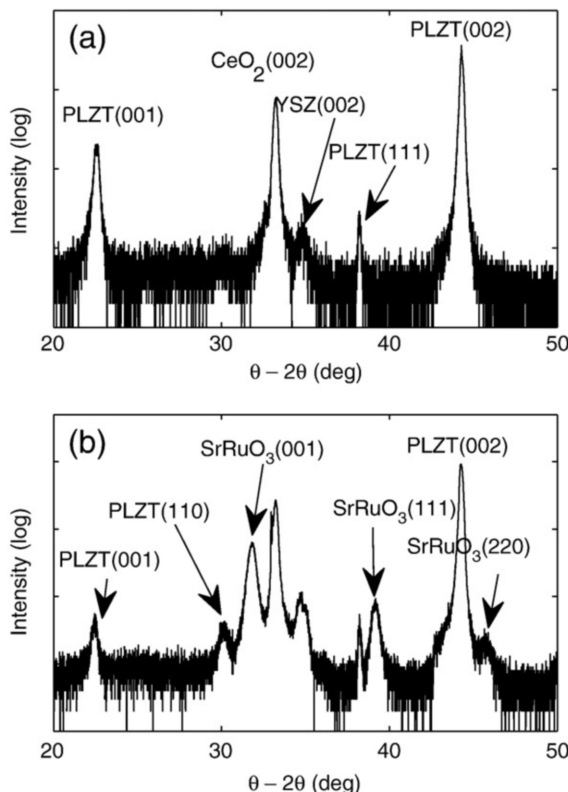

Fig 1. θ–2θ X-ray diffractograms of PLZT thin films grown on (a) CeO_2/YSZ/Si(100) and (b) $SrRuO_3$/CeO_2/YSZ/Si(100). The PLZT layer shows predominant (001) orientation in both cases.

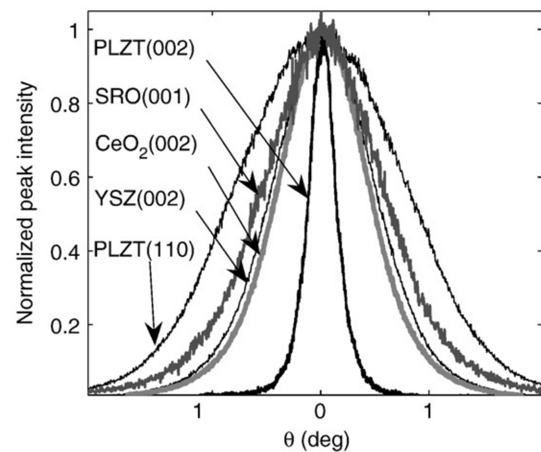

Fig. 2. Rocking curves recorded for the leading diffraction peaks of the different layers in the PLZT/$SrRuO_3$/CeO_2/YSZ thin film stack.

3. Results and discussion

Fig. 1 shows θ–2θ X-ray diffractograms for PLZT thin films grown on buffered Si(100), with and without a $SrRuO_3$ electrode layer. The scan in Fig. 1(a) pertains to a 150 nm thick film grown on CeO_2/YSZ-buffered Si(100) at a substrate temperature of 670 °C. This diffractogram shows that the e-beam deposited CeO_2 and YSZ buffer layers grow with (001) crystalline orientation, which is also the predominant orientation of PLZT. The PLZT(002) diffraction peak at $2\theta=44.4°$ corresponds to a c-axis lattice parameter 4.077 Å, close to the reported bulk value of 4.074 Å for $Pb_{0.92}La_{0.08}Zr_{0.4}Ti_{0.6}O_3$ [7], which indicates that the (001)-oriented PLZT film is relaxed. The diffractogram also reveals formation of minor domains with different crystalline orientation (cf. the PLZT(111) diffraction peak in Fig. 1(a)), which serve to accommodate the large lattice mismatch (>5%) between the PLZT and CeO_2 unit cells.

Fig. 1(b) shows the θ–2θ scan for PLZT grown on buffered Si(100) with a 20 nm $SrRuO_3$ electrode layer. This data unveils formation of more than one crystalline orientation for both PLZT and $SrRuO_3$. However, the PLZT film remains predominantly (001)-oriented. We find that a pyrochlore phase of PLZT prevails for films grown at substrate temperatures below 520 °C, as previously observed for sputter-deposited thin films on $SrTiO_3$(100) [20]. The presence of pyrochlore has been reported to degrade the dielectric and optical properties of PLZT thin films [24].

Rocking curves recorded for the leading diffraction peaks of each layer in the PLZT/$SrRuO_3$/CeO_2/YSZ thin film heterostructure are shown in Fig. 2. The rocking curves for CeO_2(002) and YSZ(002) demonstrate good crystalline quality for these e-beam deposited buffer layers, with a full width at half maximum (FWHM) of approximately 1°, in close correspondence with rocking curves previously reported for such layers [25,26]. The FWHM of the SRO

(001) rocking curve was measured at ~1.3°, and the rocking curve FWHM of the PLZT(002) and the PLZT(110) diffraction peaks were measured at 0.3° and 1.7°, respectively. Thus, the PLZT films grown on buffered Si(100) exhibit good crystalline quality for the (001)-oriented phase, with noticeably poorer quality for (110)-oriented domains. The crystalline quality of the (001)-oriented PLZT is comparable to that reported for films grown by sputter deposition on $SrTiO_3$(100) [20]. The narrower rocking curve for the PLZT(002) compared to that of the buffer layers may be attributed to the much larger thickness of the PLZT layer. The PLZT(002) rocking curve FWHM is observed to decrease with increasing thickness of the PLZT layer, due to strain relaxation. We note that the FWHM of the PLZT(002) rocking curve is not appreciably affected by introduction of a $SrRuO_3$ electrode layer in the multilayer thin film stack.

Fig. 3(a) shows φ-scans of a PLZT thin film grown directly on buffered Si(100). The fourfold rotational symmetry shows that the perovskite unit cell of PLZT is rotated 45° with respect to the CeO_2 lattice. This implies in-plane epitaxial alignment of PLZT[100] with CeO_2[110], as depicted in the sketch in Fig. 3(b). The φ-scans also show that the YSZ(111) reflections coincide with the corresponding reflections of the silicon substrate, which implies that the YSZ layer grows cube-on-cube with Si(100). Such growth is also observed for the CeO_2 layer, in agreement with the lattice alignment reported by Méchin et al. [26] and by Kondo et al. [27]. These φ-scans and the θ–2θ scans in Fig. 1 demonstrate that the PLZT films are highly oriented with a distinct in-plane alignment, and moreover, that (001)-oriented YSZ can be grown epitaxially on Si(100) without stripping the substrate of its native surface oxide prior to growth [21,28].

Fig. 4 displays typical 1×1 μm^2 AFM scans of (a) the buffered Si (100) substrate and (b) a PLZT film grown on CeO_2/YSZ/Si(100). The CeO_2 surface appears smooth, with no pronounced texture and a measured root mean square (RMS) surface roughness of ~1 nm. By comparison, the RMS roughness of the polished substrate surface was measured at ~1.5 Å for a 1×1 μm^2 scan. The RMS roughness of the PLZT film surface in Fig. 4(b) was measured at approximately 4.1 nm. This is close to the presumed upper bound on the surface roughness for propagation of light in such films with moderate optical scattering [29,30], a prerequisite for their use in optical waveguide applications. The RMS roughness of the PLZT film surface was found to increase with the film thickness, e.g. the RMS surface roughness of a PLZT film with thickness 150 nm was measured at ~1.8 nm. The PLZT film

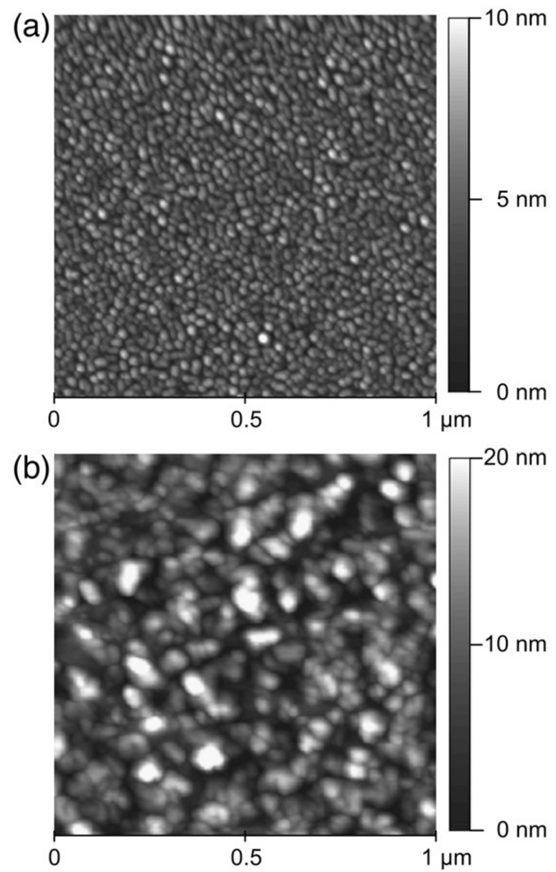

Fig. 4. 1×1 μm^2 AFM scans of (a) the e-beam evaporated CeO_2/YSZ buffer layer on Si (100) and (b) the PLZT/$SrRuO_3$/CeO_2/YSZ/Si(100) multilayer stack, with a corresponding RMS surface roughness of 1.0 nm and 4.1 nm, respectively.

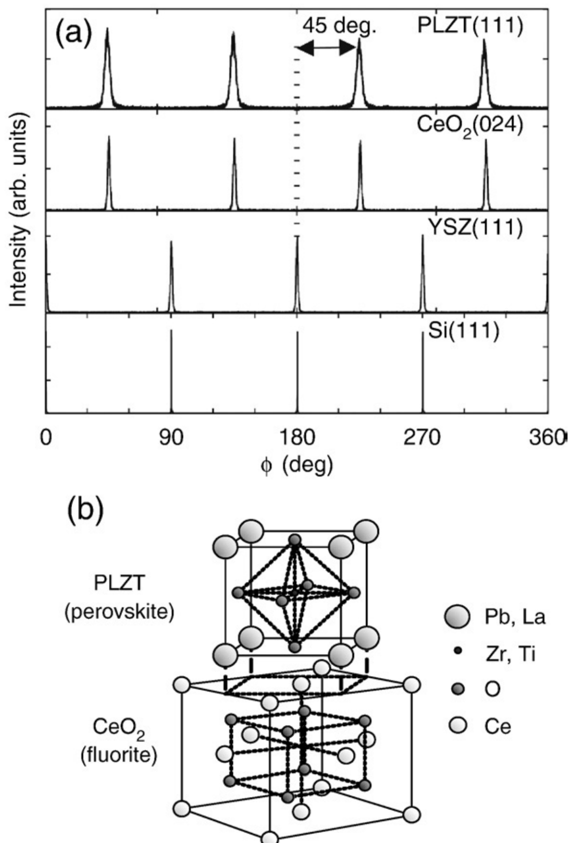

Fig. 3. (a) φ-scan diffractograms of a PLZT film grown on CeO_2/YSZ-buffered Si(100). (b) The perovskite unit cell of PLZT is rotated 45° with respect to the unit cell of CeO_2.

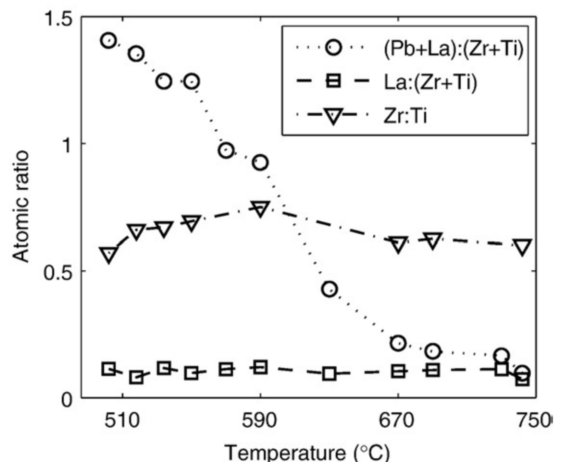

Fig. 5. Surface cation stoichiometry of PLZT films grown on CeO_2/YSZ-buffered Si(100) as a function of substrate temperature during growth.

surface appears dense and uniform with no visible voids or cracks, as measured with scanning electron microscopy. Numerical simulation of light propagation in the PLZT/$SrRuO_3$/CeO_2/YSZ/Si(100) heterostructure suggests that increasing the thickness of the dielectric buffer layers will substantially improve the confinement of horizontally propagating light to the PLZT layer [data not shown]. CeO_2 and YSZ both have a lower refractive index than PLZT, and these layers will reduce optical absorption in the semiconductor substrate if sufficiently thick. AFM analysis shows that increasing the CeO_2 layer thickness to 500 nm does not significantly affect the surface roughness of the PLZT film.

XPS data taken on the PLZT films uncovers no surface contamination beyond the presence of adventitious surface carbon. The measured Pb $4f_{7/2}$ (138.0 eV), La $3d_{5/2}$ (834.7 eV), Zr $3d_{5/2}$ (181.2 eV), and Ti $2p_{3/2}$ (458.1 eV) binding energies are in close agreement with the values previously reported for PLZT [20] and PZT [31,32]. The recorded core level spectra suggest a single oxidation state for the PLZT cations. We note that the La 3d spectra display a multiplet structure with two distinct peaks characteristic of an $a_1|3d^{-1}4f^0\rangle + a_2|3d^{-1}4f^1\underline{L}\rangle$ final state of photoemission, where $\underline{L}$ denotes a hole in a ligand O 2p orbital from charge transfer to the La 4f shell [33,34].

Fig. 5 shows the surface cation stoichiometry of sputter-deposited PLZT films vs. substrate temperature during growth, as obtained from XPS analysis. The core level peak intensities were estimated from least-squares fits of Voight lineshapes to the recorded spectra, after subtraction of a Shirley background [35]. Empirical atomic sensitivity factors [36] were used to obtain the relative cation concentrations. The plot in Fig. 5 reveals a substantial decrease in the (Pb+La):(Zr+Ti) ratio with increasing substrate temperature from 500 °C to 750 °C, while the La:(Zr+Ti) ratio remains fixed at approximately 0.1.

The loss of Pb in the film surface at high growth temperatures can be attributed to a high volatility of the Pb ions. As a result, the perovskite stoichiometry of PLZT is not preserved, which may lead to films with degraded dielectric and ferroelectric properties [37]. The target used in this experiment had 20 mol% excess Pb to compensate for the loss of Pb during growth. The XPS analysis suggests that this is not sufficient to prevent growth of Pb-depleted films for substrate temperatures above ~630 °C. The lanthanum content of the PLZT films is important both to their optical transparency and dielectric response. The optical transparency of PLZT is reported to deteriorate for material with less than 8 at.% La [7]. The measured XPS intensities (cf. Fig. 5) indicate that this should be of no concern for films grown at substrate temperatures between 500 °C and 750 °C. Moreover, the Zr:Ti ratio is found to remain fixed at approximately 40:60 for this entire temperature range, in close agreement with the target stoichiometry. The (Pb+La):(Zr+Ti) atomic ratio for PLZT films grown at higher chamber pressures (up to 150 mTorr) was also analyzed with XPS. The measurements indicate that the recorded loss of Pb is slightly diminished by increasing the oxygen partial pressure during deposition.

4. Conclusions

PLZT thin films were grown epitaxially on CeO_2/YSZ-buffered Si (100) substrate by on-axis rf magnetron sputtering. The films are preferentially (001)-oriented with a rocking curve FWHM of approximately 0.3° for the PLZT(002) diffraction peak. φ-scans show that the unit cell of PLZT is rotated 45° with respect to that of CeO_2, confirming an epitaxial relationship. Films of several hundred nanometer thickness exhibit smooth surfaces, with an RMS surface roughness of ~4 nm. The crystalline quality and surface roughness is deemed sufficient for application of such films in electro-optic and photonic devices. Quantitative XPS analysis reveals a substantial loss of Pb in the film surface and thus, a deviation from the perovskite cation stoichiometry, with increasing substrate growth temperature. In contrast, the surface concentrations of La, Zr, and Ti remain constant throughout the investigated temperature range, which holds good promise for growth of thin films with the desired dielectric response and electro-optic properties.

Acknowledgements

The authors would like to thank Erik Folven for help with the XPS measurements. This work was supported by The Research Council of Norway, under project no. 158518/431, NANOMAT nationally coordinated project “Oxides for Future Information and Communication Technology”.

References

[1] G.H. Haertling, Ferroelectrics 75 (1987) 25.
[2] J.F. Scott, Science 315 (2007) 954.
[3] R. Ramesh, H. Gilchrist, T. Sands, V.G. Keramidas, R. Haakenaasen, D.K. Fork, Appl. Phys. Lett. 63 (1993) 3592.
[4] S.G. Ghonge, E. Goo, R. Ramesh, R. Haakenaasen, D.K. Fork, Appl. Phys. Lett. 64 (1994) 3407.
[5] M. Kondo, K. Sato, M. Ishii, N. Wakiya, K. Shinozaki, K. Kurihara, Jpn. J. Appl. Phys. 45 (2006) 7516.
[6] Ø. Nordseth, T. Tybell, J. Grepstad, in: AA.S. Sudbø, G. Arisholm (Eds.), Northern Optics 2006, 2006 Northern Optics Conference Proceedings, Bergen, Norway, June 14–16, 2006, p. 51.
[7] G.H. Haertling, C.E. Land, J. Am. Ceram. Soc. 54 (1971) 1.
[8] K.H. Hardtl, D. Hennings, J. Am. Ceram. Soc. 55 (1972) 230.
[9] C.A. Copetti, H. Soltner, J. Schubert, W. Zander, O. Hollricher, Ch. Buchal, H. Schulz, N. Tellmann, N. Klein, Appl. Phys. Lett. 63 (1993) 1429.
[10] T. Wamada, N. Wakiya, K. Shinozaki, N. Mizutani, Appl. Phys. Lett. 83 (2003) 4815.
[11] N. Wakiya, T. Yamada, K. Shinozaki, N. Mizutani, Thin Solid Films 371 (2000) 211.
[12] M. Suzuki, T. Ami, Mater. Sci. Eng. B 41 (1996) 166.
[13] S. Moon, M. Kwak, Y.-T. Kim, H.-C. Ryu, S.-J. Lee, K.-Y. Kang, Int. Ferroelectr. 77 (2005) 37.
[14] H.-F. Cheng, J. Appl. Phys. 78 (1995) 4633.
[15] M. Okada, K. Tominaga, J. Appl. Phys. 71 (1992) 1955.
[16] L.L. Boyer, A.Y. Wu, G.W. Metzger, J.R. McNeil, J. Vac. Sci. Technol. A 7 (1989) 1199.
[17] E.S. Ramakrishnan, W.-Y. Howng, J. Vac. Sci. Technol. A 10 (1992) 69.
[18] J.S. Cross, M. Tomotani, Y. Kotaka, Jpn. J. Appl. Phys. 40 (2001) L346.
[19] D.S. Yoon, C.J. Kim, J.S. Lee, W.J. Lee, K. No, J. Mater. Res. 9 (1994) 420.
[20] A.K. Sarin Kumar, Ø. Dahl, S.V. Pettersen, J.K. Grepstad, T. Tybell, Thin Solid Films 492 (2005) 71.
[21] T. Hirai, K. Teramoto, H. Koike, K. Nagashima, Y. Tarui, Jpn. J. Appl. Phys. 36 (1997) 5253.
[22] S.J. Wang, C.K. Ong, L.P. You, S.Y. Xu, Semicond. Sci. Technol. 15 (2000) 836.
[23] I. Lindau, W.E. Spicer, J. Electron Spectrosc. Relat. Phenom. 3 (1974) 409.
[24] T. Nakagawa, J. Yamaguchi, T. Usuki, Y. Matsui, M. Okuyama, Y. Hamakawa, Jpn. J. Appl. Phys. 18 (1979) 897.
[25] D.K. Fork, D.B. Fenner, G.A.N. Connell, J.M. Philips, T.H. Geballe, Appl. Phys. Lett. 57 (1990) 1137.
[26] L. Méchin, J.-C. Villégier, G. Rolland, F. Laugier, Physica C 269 (1996) 124.
[27] M. Kondo, K. Maruyama, K. Kurihara, Fujitsu Sci. Tech. J. 38 (2002) 46.
[28] A. Bardal, T. Matthee, J. Wecker, K. Samwer, J. Appl. Phys. 75 (1994) 2902.
[29] B.W. Wessels, M.J. Nystrom, J. Chen, D. Studebaker, T.J. Marks, Mater. Res. Soc. Symp. Proc. 401 (1996) 211.
[30] W.J. Leng, C.R. Yang, H. Ji, J.H. Zhang, H.W. Chen, J.L. Tang, J. Appl. Phys. 100 (2006) 083505.
[31] N. Wakiya, K. Kuroyanagi, Y. Xuan, K. Shinozaki, N. Mizutani, Thin Solid Films 372 (2000) 156.
[32] J.-N. Kim, K.-S. Shin, D.-H. Kim, B.-O. Park, N.-K. Kim, S.-H. Cho, Appl. Surf. Sci. 206 (2003) 119.
[33] C. Suzuki, J. Kawai, M. Takahashi, A.-M. Vlaicu, H. Adachi, T. Mukoyama, Chem. Phys. 253 (2000) 27.
[34] T. Homna, Y. Benino, T. Fujiwara, T. Komatsu, R. Sato, V. Dimitrov, J. Appl. Phys. 91 (2002) 2942.
[35] D.A. Shirley, Phys. Rev. B 5 (1972) 4709.
[36] C.D. Wagner, L.E. Davis, M.V. Zeller, J.A. Taylor, R.H. Raymond, L.H. Gale, Surf. Interface Anal. 3 (1981) 211.
[37] M.J. Lefevre, J.S. Speck, R.W. Schwartz, D. Dimos, S.J. Lockwood, J. Mater. Res. 11 (1996) 2076.